Journal of
PERIODONTAL RESEARCH

J Periodont Res 2012; 47: 336–344

JOURNAL OF PERIODONTAL RESEARCH
doi:10.1111/j.1600-0765.2011.01438.x

# Synergistic induction of periodontal tissue regeneration by binary application of human osteogenic protein-1 and human transforming growth factor-$\beta_3$ in Class II furcation defects of *Papio ursinus*

**J. A. Teare, J.-C. Petit, U. Ripamonti**
Bone Research Unit, Medical Research Council, University of the Witwatersrand, Johannesburg, South Africa

*Teare JA, Petit J-C, Ripamonti U. Synergistic induction of periodontal tissue regeneration by binary application of human osteogenic protein-1 and human transforming growth factor-$\beta_3$ in Class II furcation defects of* Papio ursinus. *J Periodont Res 2012; 47: 336–344. © 2011 John Wiley & Sons A/S*

*Background and Objective:* Binary applications of recombinant human osteogenic protein-1 (hOP-1) and transforming growth factor-β3 (hTGF-β3) synergize to induce pronounced bone formation. To induce periodontal tissue regeneration, binary applications of hOP-1 and hTGF-$\beta_3$ were implanted in Class II furcation defects of the Chacma baboon, *Papio ursinus*.

*Material and Methods:* Defects were created bilaterally in the furcation of the first and second mandibular molars of three adult baboons. Single applications of 25 μg hOP-1 and 75 μg hTGF-$\beta_3$ in Matrigel® matrix were compared with 20:1 binary applications, i.e. 25 μg hOP-1 and 1.25 μg hTGF-$\beta_3$. Morcellated fragments of autogenous *rectus abdominis* striated muscle were added to binary applications. Sixty days after implantation, the animals were killed and the operated tissues harvested *en bloc*. Undecalcified sections were studied by light microscopy, and regenerated tissue was assessed by measuring volume and height of newly formed alveolar bone and cementum.

*Results:* The hOP-1 and hTGF-$\beta_3$ induced periodontal tissue regeneration and cementogenesis. Qualitative morphological analysis of binary applications showed clear evidence for considerable periodontal tissue regeneration. Quantitatively, the differences in the histomorphometric values did not reach statistical significance for the group size chosen for this primate study. The addition of morcellated muscle fragments did not enhance tissue regeneration. Binary applications showed rapid expansion of the newly formed bone against the root surfaces following fibrovascular tissue induction in the centre of the treated defects.

*Conclusion:* Binary applications of hOP-1and hTGF-$\beta_3$ in Matrigel® matrix in Class II furcation defects of *P. ursinus* induced substantial periodontal tissue regeneration, which was tempered, however, by the anatomy of the furcation defect model, which does not allow for the rapid growth and expansion of the synergistic induction of bone formation, particularly when additionally treated with responding myoblastic stem cells.

Ugo Ripamonti, MD, DDS, MDent, PhD, Bone Research Unit, Medical Research Council/ University of the Witwatersrand, Johannesburg, Medical School, 7 York Road, 2193 Parktown, Johannesburg, South Africa
Tel: +27 11 717 2144
Fax: +27 11 717 2300
e-mail: ugo.ripamonti@wits.ac.za

Key words: cementogenesis; osteogenic protein-1; periodontal regeneration; synergy; transforming growth factor-$\beta_3$

Accepted for publication October 10, 2011

To engineer the complex morphologies of the periodontium, the following three key components are required: an osteoinductive soluble molecular signal, an insoluble signal or substratum that acts as a scaffold for bone formation to occur, and host responding stem cells (1,2). The bone morphogenetic proteins/osteogenic proteins (BMPs/OPs) and the three mammalian transforming growth factor-β (TGF-β) proteins of the TGF-β supergene family induce endochondral bone formation in the nonhuman primate *Papio ursinus* (3), as well as periodontal tissue regeneration (4–6). Recent studies have shown that the addition of morcellated autogenous *rectus abdominis* muscle to recombinant human transforming growth factor-$\beta_3$ (hTGF-$\beta_3$) in Matrigel® matrix enhances the induction of bone formation (3,7).

Synergy, as noted by Greco *et al.* (8), is the response generated by two or more agents in which the combined effect is greater than the known effect of each agent working separately. Binary applications of recombinant human osteogenic protein-1 (hOP-1) and recombinant human transforming growth factor-$\beta_1$ (hTGF-$\beta_1$), at a ratio of 20:1 by weight, synergize to induce substantial endochondral bone formation in heterotopic intramuscular as well as orthotopic calvarial sites (9,10). The present study was designed to ascertain whether the synergistic induction of bone formation by binary applications of hOP-1 and hTGF-$\beta_3$ in Matrigel® matrix would also result in greater tissue regeneration in Class II furcation defects of *P. ursinus*.

## Material and methods

### Materials

Growth Factor Reduced Matrigel® matrix (BD Biosciences, San José, CA, USA) was used as carrier matrix for the selected morphogens. It is a soluble basement membrane extract of the Engelbreth–Holm–Swarm tumour that is liquid at 4°C and gels at 37°C to form a genuine reconstituted basement membrane (11). Recombinant human osteogenic protein-1 (hOP-1) and hTGF-$\beta_3$ were obtained from Stryker Biotech (Hopkinton, MA, USA) and Novartis AG (Basel, Switzerland), respectively.

### Primate models for tissue induction

Three clinically healthy Chacma baboons (*Papio ursinus*) with a mean weight of 16.36 ± 0.87 kg were selected from the nonhuman primate colony of the University of the Witwatersrand, Johannesburg. Criteria for selection, housing conditions and diet were as previously described (12,13). Research protocols were approved by the Animal Ethics Screening Committee of the University (clearance no. 2006/13/05). Oral hygiene procedures were carried out twice weekly until resolution of marginal gingivitis (13).

*Creation of periodontal defects* — Four Class II furcation defects were prepared bilaterally in the first and second mandibular molars of each animal as previously described (13,14; Fig. 1A). Mucoperiosteal flaps were raised, and a total of 12 furcation defects, measuring 6–8 mm in height, were surgically prepared in the first and second mandibular molars. Exposed roots were curetted to remove periodontal ligament fibres and cementum. The depth of each furcation defect measured 10–12 mm buccolingually, as measured from the buccal entrance of the exposed furcations (13–15). The surgically created defects were packed with silk suture material to expose the planed root surfaces to the oral microflora (Fig. 1B). The flaps were repositioned with resorbable sutures (Vicryl; Ethicon Inc., Somerville, NJ, USA). Postoperative pain was controlled with buprenorphine (Temgesic, Schering-Plough (Pty) Ltd., Johannesburg, South Africa), 0.01–0.03 mg/kg, intramuscular, and carprofen (Rimadyl, Pfizer Laboratories (Pty) Ltd, Johannesburg, South Africa), 2–4 mg/kg *per os*.

### Preparation of implants

Stock solutions of hOP-1 were prepared in 5 mM hydrochloric acid to a final concentration of 0.625 μg/μL, whereas hTGF-$\beta_3$ was dissolved in 20% ethanol in 100 mM acetic acid, pH 4.5. Implants were prepared in sterile 600 μL microcentrifuge tubes by adding 25 μg hOP-1or 75 μg hTGF-$\beta_3$ to a final volume of 500 μL of Matrigel® matrix. For the combination studies, 25 μg hOP-1 was added to 1.25 μg hTGF-$\beta_3$ and made up to a final volume of 500 μL with Matrigel® matrix. Previous studies in which periodontal defects were implanted with Matrigel® matrix alone showed little or no bone regeneration (5,6,15). Defects were therefore not implanted with Matrigel® matrix alone, and instead, historical control material was used for comparative data (5,6,15). All implants were kept at −70°C until implantation. At the time of surgery, harvested fragments of *rectus abdominis* muscle were morcellated with scalpel blades and added to selected binary application implants.

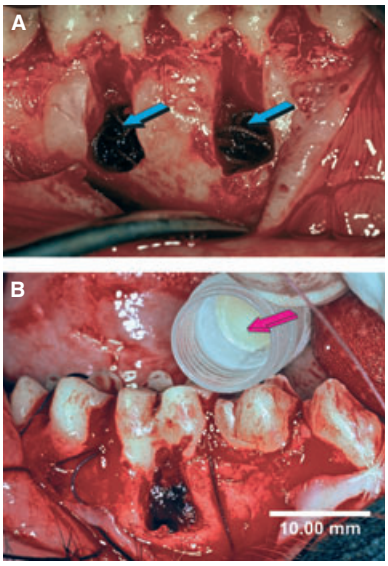


*Fig. 1.* Surgical creation and induction of Class II periodontal furcation defects in the first and second mandibular molars of the Chacma baboon, *P. ursinus*. (A) Blue arrows indicate suture material packed into the defects to encourage growth of oral microflora along the exposed root surfaces. (B) Furcation defect in a first molar, 30 d after creation, being implanted with the semi-frozen Matrigel® matrix reconstituted with recombinant morphogens (magenta arrow).

### Implantation of periodontal defects

Thirty days after creation of the furcation defects, mucoperiosteal flaps were raised and the inflammatory tissue that

had formed in the created furcation defects was debrided. The exposed root surfaces were planed and notched at the residual bony housings. The four furcation defects in each animal were implanted with Matrigel® matrix containing 25 μg hOP-1, Matrigel® matrix containing 75 μg hTGF-$\beta_3$, Matrigel® matrix with 25 μg hOP-1 and 1.25 μg hTGF-$\beta_3$ (20:1 ratio) and Matrigel® matrix with 25 μg hOP-1 and 1.25 μg hTGF-$\beta_3$ (20:1 ratio) plus morcellated autogenous muscle harvested from the *rectus abdominis*. The choices made for implantation of the devices, i.e. first or second molar, were based on surgical ease in relation to the anatomical location by implanting devices with or without morcellated muscle fragments.

The hOP-1 and hTGF-$\beta_3$ devices were implanted in a semi-frozen state, and allowed to thaw and gel within the surgically created defects, with minimal liquefaction. The mucoperiosteal flaps were realigned using resorbable sutures (Vicryl; Ethicon Inc.). Oral hygiene procedures were carried out weekly until the end of the experiment.

### Histology and histomorphometric analysis

Periodontal healing was uneventful; on the contrary, mucoperiosteal buccal swelling was noted for the hOP-1–hTGF-$\beta_3$–morcellated muscle experimental group. After 60 d, the animals were killed with an intravenous overdose of sodium pentobarbitone. Bilateral carotid 0.9% saline perfusion was followed by 10% buffered formalin perfusion. Mandibles, with surrounding soft tissue, were harvested *en bloc* and fixed in 10% buffered formalin. The specimens were processed for methylmethacrylate embedding (Fluka, Sigma-Aldrich, Seelze, Germany). Undecalcified sections were prepared by both heavy-duty microtomy (Leica Microsystems, Bensheim, Germany) and EXAKT (EXAKT Apparatebau, Norderstedt, Germany) cutting and grinding techniques (16). Histological sections prepared by heavy-duty microtomy were as previously described (13,14,17). Briefly, using a Leica SM2500E heavy-duty microtome, with 16 cm D-profile tungsten carbide knives, the polymerized blocks of periodontal tissue were trimmed along the buccal aspect until the defect orientation notches made during surgery became visible. After locating the notches, 6 μm serial sections were cut and labeled level 1 through level 100. For the ground sections, resin-embedded blocks were wet-cut by diamond-layered cutting band of the EXAKT Precision Parallel Control Cutting Unit followed by wet-grinding and polishing on the EXAKT Micro-Grinding

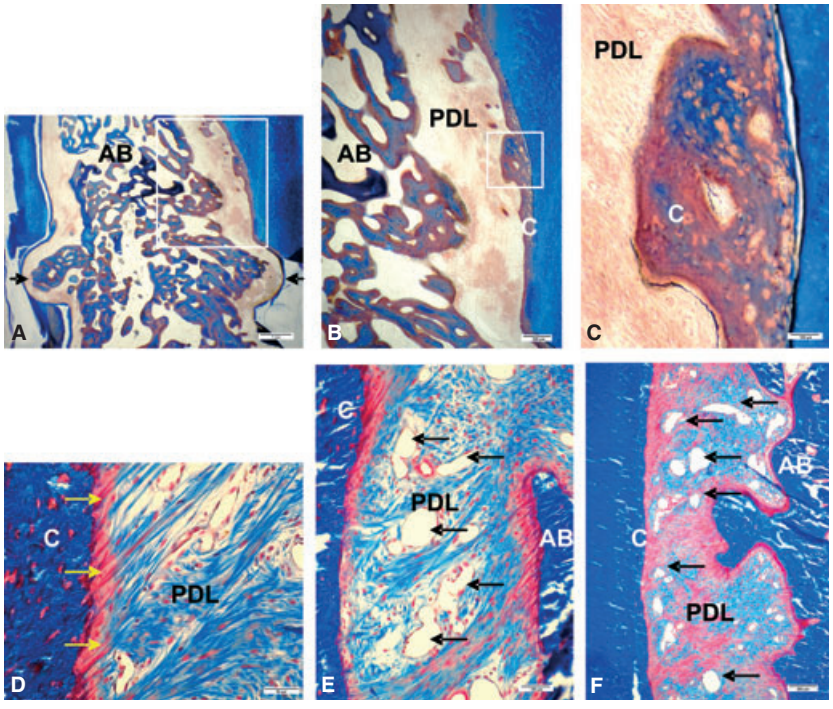


*Fig. 2.* Class II periodontal furcation defects implanted with 75 μg recombinant human transforming growth factor-$\beta_3$ (hTGF-$\beta_3$) in Matrigel® matrix. (A) Induction of alveolar bone within the defect. Black arrows indicate the notches prepared in the exposed root surfaces. Magnification ×15. (B) Inset of (A) depicting the new alveolar bone within furcation defect and the newly formed irregular, thickened cementum. Magnification × 30. (C) High-power detail of deposited thickened cementum with foci of mineralization within the cementoid matrix. Magnification ×300. (D) Insertion of functionally orientated, newly formed Sharpey's fibres (yellow arrows) into new cellular cementum. Magnification ×300. (E, F) Prominent angiogenesis (black arrows) within the newly formed periodontal ligament space. Magnification ×150 and ×75, respectively. (A–C) Undecalcified EXAKT sections, stained by modified Goldner's trichrome method. (D–F) Undecalcified Leica SM2500E section, stained by modified Goldner's trichrome method. Abbreviations: AB, alveolar bone; C, cementum; and PDL, periodontal ligament.

System to a final thickness of 15 μm using P1200 and P4000 grinding/polishing papers (18). Selected sections were stained using a modified Goldner's trichrome method for undecalcified sections. Stained sections were examined with an Olympus Provis AX70 Research Microscope (Olympus Optical Company, Tokyo, Japan).

Histological sections of the periodontal defects at levels 1 (6 μm), 50 (300 μm) and 100 (600 μm), representing the buccal, internal and central regions (one section each) of the buccal half of the defects were selected for histomorphometric analyses (15,17). Sections were evaluated for fractional volume of bone (i.e. mineralized bone and osteoid) as determined by the point counting technique (19). Using the Olympus research microscope at ×4 magnification, a 100-lattice point calibrated Zeiss Integration Platte II was superimposed over two sources (20), the apical and the coronal areas, measuring 200 lattice points per section. The height of new alveolar bone (in millimeters) in relation to total defect height at the mesial and distal aspects of each furcation defect, as well as the height of the new cementum was measured. GraphPad Prism™ (GraphPad Software Inc., La Jolla, CA, USA) computer software for statistical analyses was used to determine the mean value, the SEM and bar graphs for the variables in the analyses; *p*-values were calculated by one-way ANOVA with Bonferroni's multiple comparison test (15).

## Results

### Human transforming growth factor-$\beta_3$ (75 μg) in Matrigel® matrix

Histological sections showed new alveolar bone (Fig. 2A) within the furcation defects, as well as the formation of new cellular cementum (Fig. 2C and 2D), which appeared to be irregular and markedly thickened in some areas (Fig. 2A–C). Newly formed periodontal ligament fibres extended from the alveolar bone to the cementum (Fig. 2E and 2F), with insertion of newly formed Sharpey's fibres (yellow arrows in Fig. 2D). Most notable was the prominent vascular invasion and angiogenesis within the newly formed periodontal ligament system (Fig. 2D–F).

### Human osteogenic protein-1 (25 μg) in Matrigel® matrix

Histological sections showed new alveolar bone within the furcation defect. There were central areas of poorly vascularized, compacted collagen fibres (Fig. 3A) in the majority of sections examined. The periodontal ligament was well organized and vascularized, with functionally oriented periodontal ligament fibres inserted into alveolar bone (Fig. 3B and 3C) and newly formed cementum (Fig 3D and E).

### Binary application of 20:1 ratio hOP-1 and hTGF-$\beta_3$ in Matrigel® matrix

Histological sections showed the formation of new alveolar bone and highly vascularized mesenchymal tissues within the treated furcation defects (Fig. 4A and 4B). Periodontal ligament fibres were inserted into both

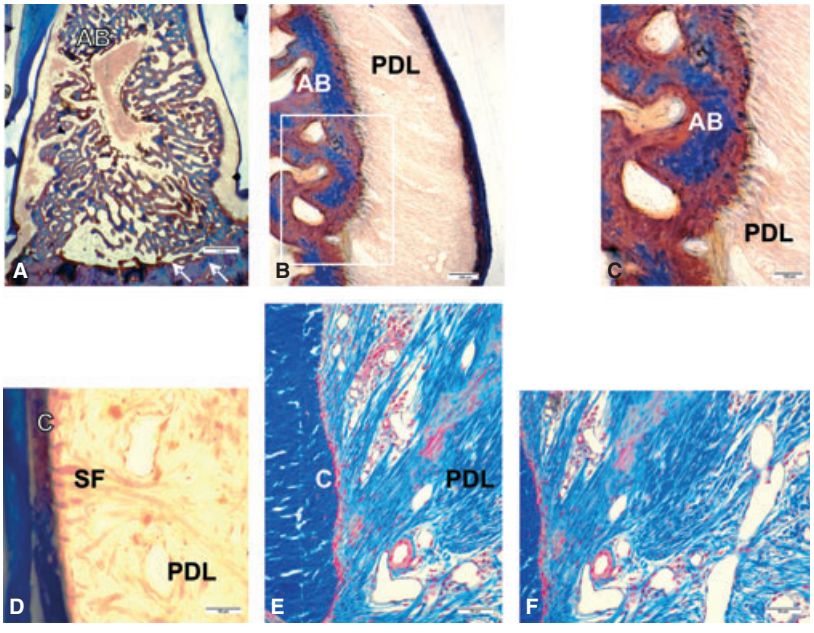


*Fig. 3.* Class II periodontal furcation defects implanted with 25 μg hOP-1 in Matrigel® matrix. (A) New alveolar bone, with compacted collagen fibres at the centre of the defect. The apical border of the remaining alveolar bone (white arrows) is shown at the base of the defect. Magnification ×15. (B, C) Newly formed periodontal ligament fibres inserting into newly formed alveolar bone. Magnification ×75 and ×150, respectively. (D) Insertion of Sharpey's fibres into new cementum. Magnification ×300. (E, F) Vascularization of the newly formed periodontal ligament. Magnification ×75. (A–D) Undecalcified EXAKT sections, stained by modified Goldner's trichrome method. (E, F) Undecalcified Leica SM2500E sections stained by modified Goldner's trichrome method. Abbreviations: AB, alveolar bone; C, cementum; PDL, periodontal ligament; and SF, Sharpey's fibres.

alveolar bone and cementum (Fig. 4C and 4E). The newly formed cementum was well defined and, in some of the sections, had filled the notch along the root surfaces (Fig. 4D and 4E). The newly formed mineralized bone was surfaced by newly deposited osteoid seams (Fig. 4F–H).

### Binary application of 20:1 ratio hOP-1 and hTGF-$\beta_3$ plus morcellated *rectus abdominis* muscle tissue in Matrigel® matrix

Postoperative healing of the periodontal defects showed pronounced swelling of the buccal mucoperiosteal flaps. The histological material showed that isolated areas of newly induced bone were restricted to the periphery of the furcation defects (Fig. 5A and 5D), with central areas of pronounced vascularization (Fig. 5A, 5B, 5D, 5E, 5G and 5H), which appeared to be propelling the alveolar bone to the outer limits of the furcation defects against the root surfaces and the mucoperiosteal flaps, as depicted at the time of tissue harvest. Deeper sections (Fig. 5D–F) revealed new alveolar bone arranged in a circular configuration, with a central vascularized area (Fig. 5D and 5E). The newly formed cementum appeared to be dense and clustered in some regions (Fig. 5C and 5F). New alveolar bone showed marked osteoid formation, which appeared to be thickened in the areas surrounding the capillaries of the invading fibrovascular tissue when compared with the osteoid of the remaining newly formed alveolar bone (Fig. 5H–J).

Comparative analyses with historical controls of Matrigel® matrix (15) showed limited bone formation when compared with the induction of bone and cementogenesis in specimens treated with hOP-1 and hTGF-$\beta_3$ in Matrigel® matrix.

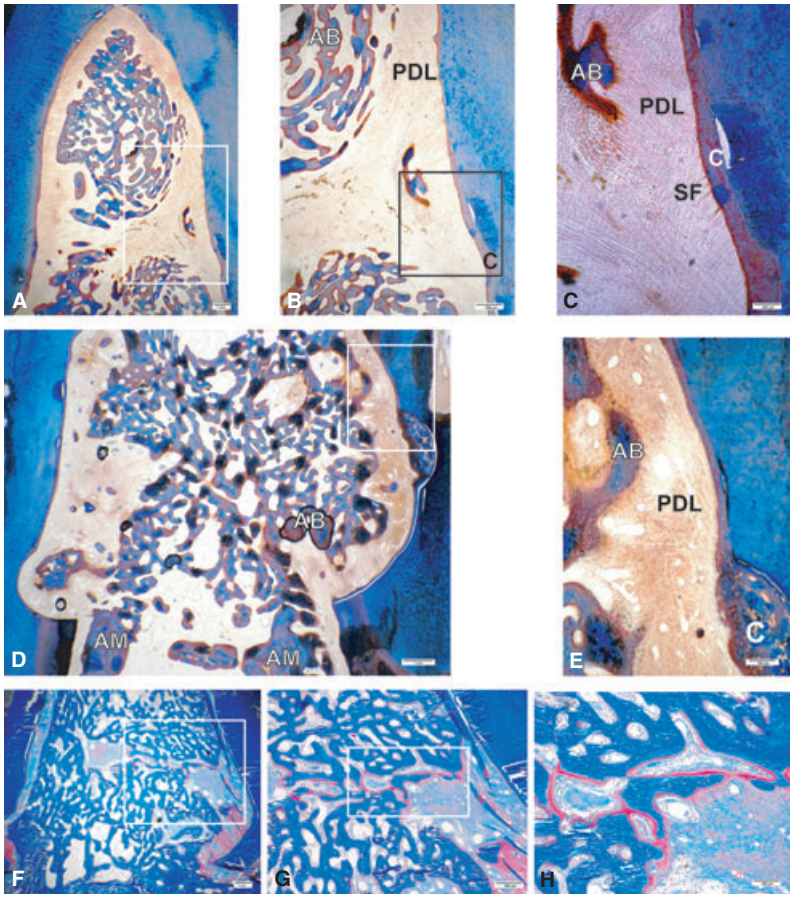


*Fig. 4.* Class II periodontal furcation defects implanted with a binary application of hOP-1 and hTGF-$\beta_3$ (20:1 ratio by weight) in Matrigel® matrix. (A, B) Newly formed alveolar bone separated by a band of collagen tissue. Magnification ×10 and ×30, respectively. (C) Newly formed periodontal ligament with insertion of Sharpey's fibres into new cementum. Magnification ×75. (D) New alveolar bone within the furcation defect and new cementum formation along mesial and distal roots. Magnification ×30. (E) High-power detail of boxed region in (D) showing alveolar bone and periodontal ligament with substantial cementogenesis within the notch. Magnification ×150. (F) Low-power view showing substantial induction of alveolar bone and cementogenesis along exposed root surfaces. Magnification ×10. (G) Medium-power detail of boxed region in (F) showing newly formed mineralized bone surfaced by osteoid seams further magnified in (H). Magnification ×30 and ×75, respectively. (A–E) Undecalcified EXAKT sections stained by modified Goldner's trichrome method. (F–H) Undecalcified Leica SM2500E sections stained by modified Goldner's trichrome method. Abbreviations: AB, alveolar bone; AM, apical margin; C, cementum; PDL, periodontal ligament; and SF, Sharpey's fibres.

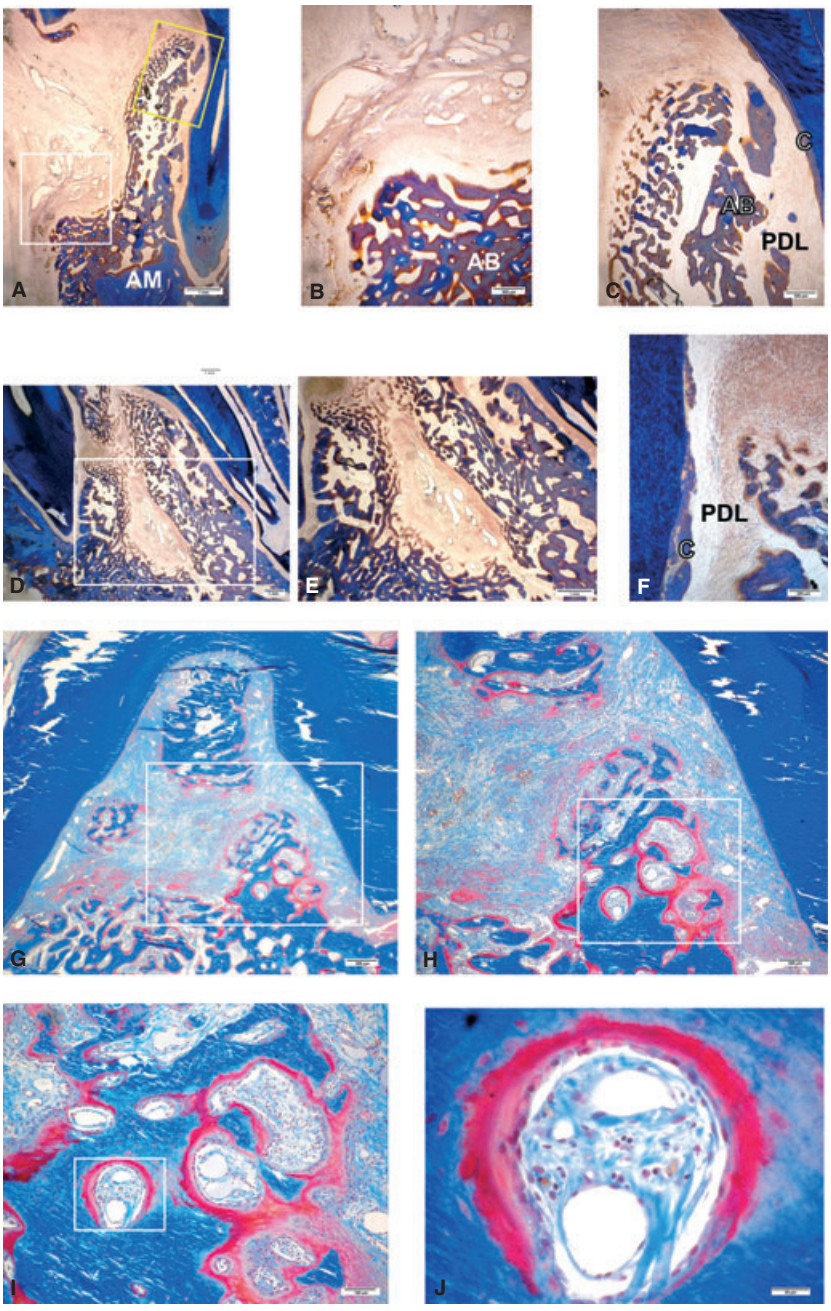


*Fig. 5.* Class II periodontal furcation defects implanted with a binary application of hOP-1 and hTGF-$\beta_3$ (20:1 ratio by weight) plus morcellated *rectus abdominis* muscle in Matrigel® matrix. (A, B) Surgically created periodontal furcation defects showing the formation of new alveolar bone along the distal root, with pronounced fibrovascular invasion; this expanding vascular tissue invasion appears to compress the alveolar bone against the root surfaces. Magnification ×15 and ×30, respectively. (C) Newly formed alveolar bone, periodontal ligament and cementum. Magnification ×30. (D, E) Deeper cut section showing the concentric anatomical disposition of the newly formed alveolar bone within the confines of the furcation defect, with a central area of highly vascularized fibrovascular tissue. Magnification ×10 and ×15, respectively. (F) New alveolar bone, periodontal ligament and irregular, thickened cementum. Magnification ×75. (G–J) New alveolar bone and pronounced osteoid deposition surrounding newly formed capillaries. Magnification ×30, ×75, ×150 and ×300, respectively. (A–F) Undecalcified EXAKT sections stained by modified Goldner's trichrome method. (G–J) Undecalcified Leica SM2500E sections stained by modified Goldner's trichrome method. Abbreviations: AB, alveolar bone; AM, apical margin; C, cementum; PDL, periodontal ligament; and SF, Sharpey's fibres.

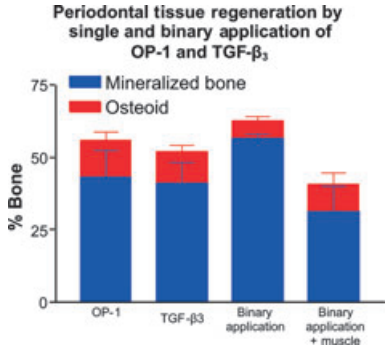


*Fig. 6.* Distribution of alveolar bone (mineralized bone plus osteoid) as regenerated by each of the four treatments. Periodontal tissue regeneration by binary application of hOP-1 and hTGF-$\beta_3$ in Matrigel® matrix yielded a considerable amount of alveolar bone (62.67 ± 1.94%) compared with single applications of hOP-1 (55.85 ± 9.19%) and hTGF-$\beta_3$ (52.15 ± 5.33%). Binary application of hOP-1 and hTGF-$\beta_3$ with the addition of morcellated autogenous muscle yielded the least alveolar bone (40.76 ± 7.39%). There were no significant differences ($p > 0.05$) between treatments, as calculated by Bonferroni's multiple comparison test.

### Histomorphometric analysis

Figure 6 shows the volume of newly formed mineralized and osteoid generated by the four implant modalities. The largest amount of alveolar bone was generated by the binary application of hOP-1 and hTGF-$\beta_3$ in Matrigel® matrix (62.67 ± 1.94%). The difference in the values, however, was not significant. Single applications of hTGF-$\beta_3$ and hOP-1 also resulted in substantial induction of bone formation, 52.15 ± 5.33 and 55.85 ± 9.19%, respectively. Binary applications combined with morcellated *rectus abdominis* muscle showed smaller amounts of mineralized bone (40.76 ± 7.39%), but with prominent osteoid synthesis when compared with hTGF-$\beta_3$ and hOP-1 applied singly (Fig. 5); this difference, however, was not significant.

Table 1 gives the linear measurements (means ± SEM in millimeters) of the regenerated alveolar bone and cementum along the exposed root surfaces for the height of the defect from the notch to the fornix of the furcation (N-F), the height of the new cementum (N-C) and new alveolar bone (N-AB). Significant differences ($p < 0.01$) were noted for the linear measurement of the mesial cementum (N-C) for TGF-$\beta_3$ single application vs. binary application combined with morcellated muscle, and binary application vs. binary application combined with morcellated fragments of *rectus abdominis* muscle.

## Discussion

The present study has shown that single applications of hOP-1 and hTGF-$\beta_3$ induce periodontal tissue regeneration in Class II furcation defects of the nonhuman primate *P. ursinus*. When the two morphogens are combined, a synergy is created, resulting in substantial tissue induction (9,10). Although the difference in histomorphometric values was not statistically significant, the morphological analyses of the treated specimens showed important morphological differences of tissue induction and morphogenesis. Recombinant hOP-1 and hTGF-$\beta_3$ synergistically interacted to construct the regenerated tissues with newly formed alveolar bone displaced against the exposed root surfaces. This was due to the prominent angiogenesis generated by the synergistic induction of bone formation in intimate contact with the newly formed osteoid matrix (Fig. 5H–J). To the best of our knowledge, this is the first periodontal study that shows effective synergistic interactions between binary morphogen applications.

Single applications of hOP-1 and hTGF-$\beta_3$ generated similar amounts of mineralized bone within the furcation defects. Prominent vascularization of the periodontal ligament was sufficiently demonstrated by both proteins, which is indicative of their angiogenic properties (5,15,21,22). Furthermore, newly formed cementum was well represented, particularly within the hTGF-$\beta_3$-implanted defects

*Table 1.* Histometric analysis of periodontal tissue regeneration in furcation defects

| | hTGF-$\beta_3$ alone | SEM | *n* | hOP-1 alone | SEM | *n* | Binary application | SEM | *n* | Binary application + muscle | SEM | *n* |
|---|---|---|---|---|---|---|---|---|---|---|---|---|
| Mesial | | | | | | | | | | | | |
| N-F | 7.37 | ± 0.56 | 6 | 6.83 | ± 0.63 | 6 | 7.06 | ± 0.32 | 6 | 5.31 | ± 0.45 | 6 |
| N-C | 5.13* | ± 0.47 | 6 | 3.44 | ± 0.95 | 6 | 5.03* | ± 0.73 | 6 | 0.90 | ± 0.51 | 6 |
| N-AB | 6.78 | ± 0.65 | 6 | 5.60 | ± 1.23 | 6 | 6.79 | ± 0.35 | 6 | 2.70 | ± 1.11 | 6 |
| Distal | | | | | | | | | | | | |
| N-F | 7.28 | ± 0.54 | 6 | 6.91 | ± 0.61 | 6 | 7.44 | ± 0.63 | 6 | 6.32 | ± 1.04 | 6 |
| N-C | 6.18 | ± 0.33 | 6 | 3.65 | ± 0.88 | 6 | 5.45 | ± 0.89 | 6 | 2.69 | ± 1.06 | 6 |
| N-AB | 5.93 | ± 0.92 | 6 | 5.67 | ± 1.17 | 6 | 7.07 | ± 0.57 | 6 | 4.73 | ± 1.08 | 6 |

Values (in millimeters) are given as means ± SEM; *n* indicates the number of sections per implant type measured. Abbreviations: AB, alveolar bone; C, cementum; F, fornix of the furcation defect; hOP-1, human osteogenic protein-1; hTGF-$\beta_3$, recombinant human transforming growth factor-$\beta_3$; N, apical border of the notches on mesial and distal root surfaces; and *n*, number of histological sections counted. Significant differences (*$p < 0.01$), as detected by Bonferroni's multiple comparison test, were noted for the linear measurement of the mesial cementum (N-C) for hTGF-$\beta_3$ single application vs. binary application combined with muscle, and binary application vs. binary application combined with muscle.

(Fig. 2A–C). Interestingly, previous studies have shown hOP-1 to be highly cementogenic (6,23,24). Cementogenesis generated by hTGF-$\beta_3$, as seen in this study, was also substantial, but not statistically significantly greater ($p > 0.05$) than that produced by hOP-1 (Table 1). Further investigation of the cementogenic properties of these two proteins is therefore indicated, particularly by studying the morphology and the width of the newly deposited cementum.

Binary application of 20:1 hOP-1 and hTGF-$\beta_3$ engineered more alveolar bone by volume than single applications of each individual recombinant morphogen (Fig. 6). This difference, however, was not statistically significant ($p > 0.05$). The newly formed cementum, although conspicuous throughout the furcation defect, especially within the notches (Fig. 4D and 4E), did not exceed the amount of cementum induced by hTGF-$\beta_3$ applied singly. In general, the periodontal ligament fibres appeared to be functionally inserted into the new alveolar bone and new cementum. Morphological observations suggested that single, rapidly forming ossicles may have been initiated within the implanted furcations, each separated by highly vascularized mesenchymal tissue. Sections showed the merging of the different osteogenetic areas (Fig. 4F and 4G).

Binary application of hOP-1 and hTGF-$\beta_3$ together with morcellated autogenous *rectus abdominis* muscle did not result in greater periodontal tissue regeneration (Fig. 6). Previously, we have shown that the addition of morcellated autogenous *rectus abdominis* muscle enhances the inductive capacity of the hTGF-$\beta_3$ isoform (3,5–7,15). However, upon morphological examination of the treated defect, the new alveolar bone appeared to be restricted to the periphery of the defect, with an inner core of highly vascularized tissue (Fig. 5G and 5H). Histological sections taken deeper into the defect, beyond the core of soft tissue, showed increased bone formation, with a lesser amount of vascularized mesenchymal tissue. In earlier studies investigating the synergistic induction of bone formation (9,10), the dynamic pace and volume of bone induction by binary applications of TGF-$\beta_1$ isoform and hOP-1 induced a pronounced tissue displacement within the implanted *rectus abdominis* muscle and cranial defects (9,10). The postoperative swelling noted along the buccal mucoperiosteal flap may be indicative of such dynamic events occurring within the restricted environment of a Class II furcation defect. There was an abundance of newly formed osteoid, which appeared to be intimately associated with blood vessels (Fig. 5H–J). Indeed, the endothelial cells appeared to be virtually in physical contact with the osteoid seams, highlighting the concept that angiogenesis is a prerequisite for osteogenesis (25–27).

Thickened and irregular formation of the newly formed cementum was common to defects implanted with hTGF-$\beta_3$; the cementum, as induced by hOP-1, appeared to be of a consistent, uniform width across the exposed root surfaces (Fig. 3A and 3B). Cementogenesis, as initiated by hTGF-$\beta_3$ applied singly or combined with hOP-1, was pronounced along the treated root surfaces, with occasional large masses extending into the periodontal ligament space (Fig. 2B and 2C, Fig. 4D and 4E and Fig. 5F).

In conclusion, in Class II furcation defects of the nonhuman primate *P. ursinus*, binary applications of hOP-1 and hTGF-$\beta_3$ induced considerable amounts of mineralized bone and osteoid; however, the addition of morcellated *rectus abdominis* muscle containing myoblastic stem cells limited the induction of alveolar bone. Within the limits of the presented morphological analyses, the confined, nonexpandable Class II furcation defects profoundly limited tissue induction and morphogenesis initiated by the synergistic induction of bone formation as classically shown in heterotopic sites of the *rectus abdominis* muscle and orthotopic sites of the calvaria, which allowed for rapid expansion of the newly formed ossicles (9,10). The number of animals used was yet another limitation for this study, and although the focus is to evaluate the experimental data statistically, morphology is the first analytical parameter. Qualitative morphological analysis of binary applications showed clear evidence for substantial periodontal tissue regeneration. Quantitatively, the difference in histomorphometric values did not reach statistical significance for the group size chosen. The study, however, provides new data on the cementogenic and angiogenic activities of TGF-$\beta_3$, when delivered by Matrigel® matrix, in Class II furcation defects of the nonhuman primate *P. ursinus*.

## Acknowledgements

This work is supported by the South African Medical Research Council, the University of the Witwatersrand, Johannesburg, and the National Research Foundation. We thank Stryker Biotech for the supply of the recombinant human osteogenic protein-1 and Novartis AG for the recombinant human transforming growth factor-$\beta_3$. Special thanks to Mrs Ruqayya Parak for histological techniques and Dr Cinda Cupido for insightful observations and support.

## References

1. Reddi AH. Morphogenesis and tissue engineering of bone and cartilage: inductive signals, stem cells, and biomimetic biomaterials. *Tissue Eng* 2000;**6:**351–359.
2. Ripamonti U, van den Heever B, Crooks J *et al*. Long-term evaluation of bone formation by osteogenic protein 1 in the baboon and relative efficacy of bone-derived bone morphogenetic proteins delivered by irradiated xenogeneic collagenous matrices. *J Bone Miner Res* 2000;**15:**1798–1809.
3. Ripamonti U, Ferretti C, Teare J, Blann L. Transforming growth factor-β isoforms and the induction of bone formation: implications for reconstructive craniofacial surgery. *J Craniofac Surg* 2009;**20:** 1544–1555.
4. Ripamonti U, Reddi AH. Tissue engineering, morphogenesis, and regeneration of the periodontal tissues by bone morphogenetic proteins. *Crit Rev Oral Biol Med* 1997;**8:**154–163.
5. Ripamonti U, Parak R, Petit JC. Induction of cementogenesis and periodontal ligament regeneration by recombinant human transforming growth factor-$\beta^3$ in Matrigel with rectus abdominis responding cells. *J Periodont Res* 2009;**44:**81–87.

6. Ripamonti U, Petit JC, Teare J. Cementogenesis and the induction of periodontal tissue regeneration by the osteogenic proteins of the transforming growth factor-β superfamily. *J Periodont Res* 2009;**44:**141–152.
7. Ripamonti U, Ramoshebi LN, Teare J, Renton L, Ferretti C. The induction of endochondral bone formation by transforming growth factor-$\beta_3$: experimental studies in the non-human primate *Papio ursinus*. *J Cell Mol Med* 2008;**12:**1029–1048.
8. Greco WR, Faessel H, Levasseur L. The search for cytotoxic synergy between anticancer agents: a case of Dorothy and the ruby slippers? *J Natl Cancer Inst* 1996;**88:**699–700.
9. Ripamonti U, Duneas N, van den Heever B, Bosch C, Crooks J. Recombinant transforming growth factor-$\beta_1$ induces endochondral bone in the baboon and synergizes with recombinant osteogenic protein-1 (bone morphogenetic protein-7) to initiate rapid bone formation. *J Bone Miner Res* 1997;**12:**1584–1595.
10. Duneas N, Crooks J, Ripamonti U. Transforming growth factor-$\beta_1$: induction of bone morphogenetic protein genes expression during endochondral bone formation in the baboon, and synergistic interaction with osteogenic protein-1 (BMP-7). *Growth Factors* 1998;**15:**259–277.
11. Kleinman HK, McGarvey ML, Hassell JR *et al*. Basement membrane complexes with biological activity. *Biochemistry* 1986;**25:**312–318.
12. Ripamonti U. Bone induction in nonhuman primates. An experimental study on the baboon. *Clin Orthop Relat Res* 1991; **269:**284–294.
13. Ripamonti U, Heliotis M, van den Heever B, Reddi AH. Bone morphogenetic proteins induce periodontal regeneration in the baboon (*Papio ursinus*). *J Periodont Res* 1994;**29:**439–445.
14. Ripamonti U, Heliotis M, Rueger DC, Sampath TK. Induction of cementogenesis by recombinant human osteogenic protein-1 (OP-1/BMP-7) in the baboon (*Papio ursinus*). *Arch Oral Biol* 1996; **41:**121–126.
15. Teare JA, Ramoshebi LN, Ripamonti U. Periodontal tissue regeneration by recombinant human transforming growth factor-$\beta_3$ in *Papio ursinus*. *J Periodont Res* 2008;**43:**1–8.
16. Donath K, Breuner G. A method for the study of undecalcified bones and teeth with attached soft tissues. The Sage-Schliff (sawing and grinding) technique. *J Oral Pathol* 1982;**11:**318–326.
17. Ripamonti U, Crooks J, Teare J, Petit J-C, Rueger DC. Periodontal tissue regeneration by recombinant human osteogenic protein-1 in periodontally-induced furcation defects of the primate *Papio ursinus*. *S Afr J Sci* 2002;**99:**361–368.
18. Ripamonti U, Klar RM, Renton LF, Ferretti C. Synergistic induction of bone formation by hOP-1, hTGF-$\beta_3$ and inhibition by zoledronate in macroporous coral-derived hydroxyapatites. *Biomaterials* 2010;**31:**6400–6410.
19. Parfitt AM. Stereologic basis of bone histomorphometry: theory of quantitative microscopy and reconstruction of third dimension. In: Recker HR, ed. *Bone Histomorphometry: Techniques and Interpretatio*. Boca Raton: CRC Press, 1983:53–87.
20. Parfitt AM, Drezner MK, Glorieux FH *et al*. Bone histomorphometry: standardization of nomenclature, symbols, and units. Report of the ASBMR Histomorphometry Nomenclature Committee. *J Bone Miner Res* 1987;**2:**595–610.
21. Yeh LC, Lee JC. Osteogenic protein-1 increases gene expression of vascular endothelial growth factor in primary cultures of fetal rat calvaria cells. *Mol Cell Endocrinol* 1999;**153:**113–124.
22. Ramoshebi LN, Ripamonti U. Osteogenic protein-1, a bone morphogenetic protein, induces angiogenesis in the chick chorioallantoic membrane and synergizes with basic fibroblast growth factor and transforming growth factor-$\beta_1$. *Anat Rec* 2000;**259:**97–107.
23. Ripamonti U, Crooks J, Petit JC, Rueger DC. Periodontal tissue regeneration by combined applications of recombinant human osteogenic protein-1 and bone morphogenetic protein-2. A pilot study in Chacma baboons (*Papio ursinus*). *Eur J Oral Sci* 2001;**109:**241–248.
24. Ripamonti U, Petit JC. Bone morphogenetic proteins, cementogenesis, myoblastic stem cells and the induction of periodontal tissue regeneration. *Cytokine Growth Factor Rev* 2009;**20:**489–499.
25. Trueta J. The role of vessels in osteogenesis. *J Bone Joint Surg* 1963;**45B:**402–418.
26. Kaigler D, Krebsbach PH, West ER *et al*. Endothelial cell modulation of bone marrow stromal cell osteogenic potential. *FASEB J* 2005;**19:**665–667.
27. Kaigler D, Krebsbach PH, Wang Z *et al*. Transplanted endothelial cells enhance orthotopic bone regeneration. *J Dent Res* 2006;**85:**633–637.